Magnetic Performance Assessment of the S-PRESSO Superconducting Undulator Mock-Up

Johann E. Baader, Sara Casalbuoni, Vanessa Grattoni, Andreas Grau, Achim Hobl, Alexander Vatagin, Mikhail Yakopov, and Paweł Ziółkowski

***Abstract*—Superconducting undulators constitute an important element of the European XFEL facility development program. The application of SCU technology at European XFEL paves the way to potentially enable lasing above 50 keV, opening new frontiers in scientific research and offering unprecedented capabilities in high-energy applications. A total of six modules are foreseen. The Superconducting undulator PRE-SerieS mOdule (S-PRESSO) is the preseries module for the free-electron laser superconducting undulator afterburner. This article presents a comprehensive assessment of the S-PRESSO superconducting undulator mock-up's magnetic performance conducted at the Institute for Beam Physics and Technology of the Karlsruhe Institute of Technology. After a description of the experimental setup and the coil, the results of training and of the magnetic field measurements are presented. The results demonstrate a robust design of the mock-up, which achieved the short sample limit, a long lasting stability at nominal current tested for 8 h, and a straight trajectory below European XFEL requirements. The measured quality of the magnetic field is studied and compared with simulations using the geometric values measured at room temperature with a coordinate measuring machine. This analysis suggests areas for potential improvement in the manufacturing process.**

***Index Terms*—Cryostats, magnetic field measurements, superconducting coils, undulators.**

I. Introduction

IN THE evolving landscape of photon science, synchrotron light sources and free-electron lasers (FELs) have emerged as indispensable tools, driving breakthroughs across disciplines ranging from materials science to biological imaging. Central to their capabilities is the quality and characteristics of the generated radiation beams. Compared with standard permanent magnet-based undulators, superconducting undulators (SCUs) play a pivotal role in this context, offering distinct advantages over traditional undulator designs [1]. Characterized by their ability to produce higher magnetic fields for short periods, SCUs allow achieving higher photon energies with lower electron beam energies. Institutes, such as SLAC National Accelerator Laboratory [2], Shanghai Advanced Research Institute [3], and European XFEL, are working on the integration of SCUs into their FEL facilities, reflecting a focused move toward harnessing these advanced systems.

European XFEL foresees the implementation of SCUs as part of its facility development program [4]. Five SCU units and a prototype module named Superconducting undulator PRE-SerieS mOdule (S-PRESSO) are proposed to be integrated into the existing SASE2 hard X-rays beamline. The S-PRESSO module houses two SCU coils, each 2 m in length, accompanied by superconducting corrector coils wrapped around the final grooves of the iron yoke. In addition, it includes two sets of iron-free coils, one vertical and one horizontal, positioned amidst the primary coils, with a superconducting phase shifter situated between these pairs. The period and magnetic gap are 18 and 6.5 mm, respectively, with an on-axis peak field of 1.82 T [5]. The contract for the production of S-PRESSO has been given to Bilfinger Noell GmbH.

Two magnetic measurement stations are being established at European XFEL. One, designated SUNDAE1 (Superconducting UNDulAtor Experiment 1) [6], will be employed to inspect the superconducting coils up to two meters in a vertical helium bath cryostat. SUNDAE2 will be developed to perform in-vacuum magnetic field measurements of SCUs in the final cryostat [7].

In this study, we aim to evaluate the manufacturing and assembly quality of the S-PRESSO coils by characterizing a 300 mm-long mock-up using advanced magnetic measurement techniques. At the Institute for Beam Physics and Technology (IBPT) Karlsruhe Institute of Technology (KIT), the mock-up was installed and measured at the CASPER I facility [8], using a sledge (where the Hall probe is placed) developed by European XFEL. The measurements have been used to characterize the mock-up's magnetic field and to validate the sledge system, ensuring its readiness for installation in the SUNDAE1 test stand.

The rest of this article is organized as follows. Section II focuses on the experimental setup. Section III describes the S-PRESSO mock-up, including its main specifications and the magnetic simulations. Section IV shows the measurement results. Finally, Section V presents the conclusions. We refer to the magnetic flux density (also known as magnetic induction) B as "magnetic field" or simple "field" throughout this article.

Manuscript received 21 December 2023; revised 29 February 2024 and 15 April 2024; accepted 15 April 2024. Date of publication 18 April 2024; date of current version 30 April 2024. *(Corresponding author: Johann E. Baader.)*

Johann E. Baader, Sara Casalbuoni, Vanessa Grattoni, Mikhail Yakopov, and Paweł Ziółkowski are with European XFEL, 22869 Schenefeld, Germany (e-mail: johann.baader@xfel.eu).

Andreas Grau is with the Karlsruhe Institute of Technology, 76344 Karlsruhe, Germany.

Achim Hobl and Alexander Vatagin are with Bilfinger Noell GmbH, 97080 Würzburg, Germany.

Color versions of one or more figures in this article are available at https://doi.org/10.1109/TASC.2024.3390929.

Digital Object Identifier 10.1109/TASC.2024.3390929

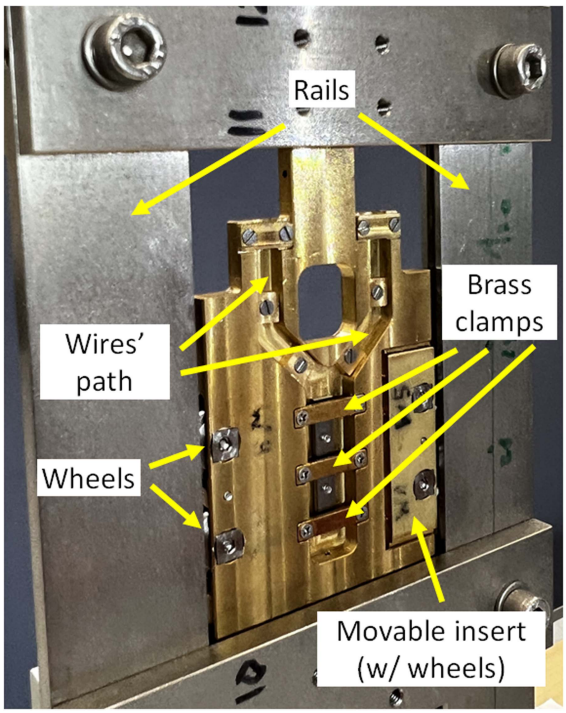

Fig. 1. Sledge set in precisely machined rails. The Hall probe, not shown in the picture, is firmly fixed underneath the brass clamp. Adapted from [4].

II. Experimental Setup

CASPER I serves as a vertical liquid helium bath cryostat test stand for evaluating SCU coils up to approximately 350 mm long with a measurement distance for field characterization of about 500 mm [8]. Designed cylindrically, it boasts an internal diameter of 370 mm. A heating element and temperature gauge sit at its base to facilitate the evaporation of liquid helium, which is recovered. Placed outside (above) the cryostat, an independent linear mover controls a shaft with a precision of 1 μm. The shaft is linked to a sledge with a Hall probe measuring the magnetic field profile along the magnetic axis of the undulator coils. The Hall sample voltage data are taken by a Keithley DAQ system and the sledge position data are gained by a linear encoder. For the power supplies and feedthroughs up to 2500 A, quench detectors and a quench diagnostic system for 32 channels are available.

The sledge that houses the Hall probe was designed at European XFEL, and it is shown in Fig. 1. The sledge is made of brass, fitting a minimum 5 mm magnetic gap between the coils. Titanium wheels drive the sledge through a specially designed rail assembled between the coils and used as a spacer. The sledge has a movable insert pushed by four compression springs to guarantee the Hall probe's position stability during the scan.

The position of the hall probe was checked before installation into the cryostat insert. This was done on a granite table using two prototypes of the rails and a mechanical gauge. The rails are manufactured to define the gap within 10 μm at room temperature. The measuring setup was oriented horizontally, which relatively gives the maximum displacement between the Hall probe's position against the left and right rail. The position

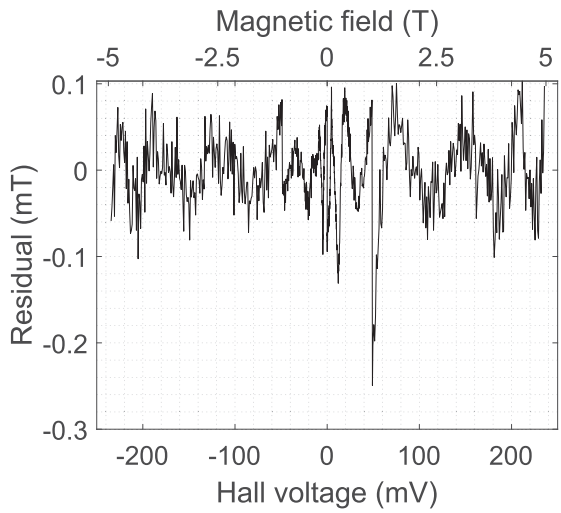

Fig. 2. Calibration error of the Hall probe used for the measurements.

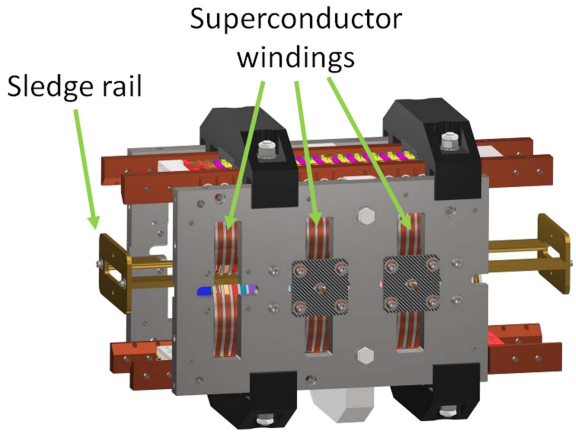

Fig. 3. CAD model of the S-PRESSO mock-up.

oscillation of the fully assembled sledge stayed within 40 μm, below the specified 100 μm.

A cryogenic Hall probe was used for the test. The Hall probe has been calibrated at the Institute of Technical Physics at KIT inside a physical property measurement system operating at 4 K from the company Quantum Design. The calibration error, predominantly within 0.1 mT with a maximum deviation of 0.25 mT (likely an outlier during the calibration), reflects the accuracy of the polynomial fit relative to the original data. The Hall probe operates under a nominal current of 10 mA, has a sensitivity of 49.6 mV/T, and its active area dimension is 50 μm $\times$ 50 μm. Fig. 2 shows the calibration error curve of the Hall probe used, defined as the difference (also called Residual) between the reference field and the results from the polynomial fit.

III. S-PRESSO Mock-Up

A. Mock-Up Design

Fig. 3 shows the mock-up CAD model. The mock-up, at a length of 300 mm, serves as a scaled-down segment of the S-PRESSO with the same period length of 18 mm and magnetic

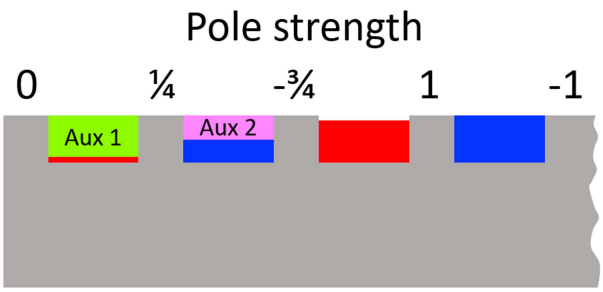

Fig. 4. Schematic representation of the end windings. The main coil winding is in blue and red, Aux 1 in green, and Aux 2 in purple.

gap of 6.5 mm. The same geometry of the iron yoke incorporates the same end field design including superconducting corrector coils positioned in the final grooves.

The mock-up undulator magnetic field is point-symmetric (antisymmetric configuration), designed for 14 full periods. The pure iron core's winding yokes require a total of 34 poles and 33 winding grooves to include the end field compensation. The nominal pole width and height are 3.46 and 9.45 mm, respectively [4]. The end field compensation is achieved by installing a different winding package in the final three grooves on each side of the SCU coils. This adjustment modifies the relative pole strength to 0, 1/4, −3/4, 1, −1, 1, and so on, which minimizes the field integrals. The end field compensation together with the end field corrector coils, called "Aux 1" and "Aux 2," are shown in Fig. 4.

The auxiliary correction coils are wound on top of the main coil in the last two winding grooves using a 0.254 mm diameter wire (including insulation). These correction coils allow trimming the end field adaption over the full range of operating currents, which is needed to compensate the effects of the iron nonlinearity to provide field integral correction.

The shape of the main coils is composed of a 65 mm long straight section on the side facing the electron beam to ensure a low field roll-off, and a smaller radius section connecting to the back side, which is closed by a half-circle.

The superconducting wire is wound in grooves machined into the iron core. Each groove is insulated on the sides and the groove's inner surface. To attain the undulator field pattern, the winding direction is changed between each two consecutive winding grooves. Each main coil groove houses 11 layers with 5 turns/layer for a total of 55 turns per groove. A rectangular NbTi superconducting multifilamentary wire is used for the main coil grooves. Bare dimensions are 0.6 mm high by 1 mm wide with a filament diameter of 13 μm. The conductor operates at 86% of the 4.2 K short sample limit with a current sharing temperature of 5.22 K. The temperature margin is 1.02 K concerning the design temperature of 4.2 K, as shown in Fig. 5.

The SCU is designed to operate in conduction cooling, to be later integrated into a cryogen-free cryostat. The coils have been impregnated after winding and inserted into a stabilizing mechanical structure that ensures tight magnetic gap dimensions by precisely machined spacers. The rails for guiding the Hall probe sledge have been integrated into the structure.

Two figures that are important to evaluate the field's quality are the root mean square (rms) and the range of half-K parameter

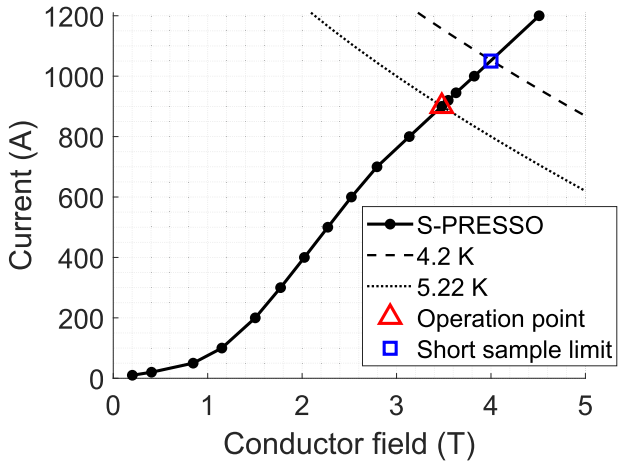

Fig. 5. Loadline of S-PRESSO coils. The blue square shows the point where the loadline crosses the critical current at 4.2 K (short sample limit). The dashed line is the critical current from the manufacturers at 4.2 K and the dotted line represents a fit curve using the Bottura parameterization [9]. The operating point is 900 A, 1.845 T on-axis, and 3.48 T on the conductor, denoted by the red triangle. The current sharing temperature is 5.22 K and the conductor is operating at 86% of the 4.2 K short sample limit.

relative change. For S-PRESSO, the specified numbers for the rms and range are 1.5×10^{-3} and $\pm 6 \times 10^{-3}$, respectively [10].

B. Simulation Description

Simulations with the software Opera3D [11] have been performed to calculate the loadline shown in Fig. 5. As proved in the measurements described in the following sections, the mock-up reached the short sample limit (see the blue square marker in Fig. 5).

The quality of the magnetic field is strictly related to the mechanical accuracies reached in manufacturing the coils and to the precision with which the coils are assembled together (magnetic gap). In particular, the deviations from the nominal values of the pole and groove widths, and pole and winding heights are measured at room temperature with a coordinate measuring machine. These measurements are used to build the geometry in simulations performed with FEMM [12], assuming no error in the magnetic gap. The measured and specified values of the mechanical accuracies reached for both coils are shown in Fig. 6.

The winding height was measured for only one of the coils. Being this below 5 μm, for the other coil the winding height has been assumed to be ideal. For the end field configuration, the geometry shown in Fig. 4 has been used. The magnetic field on-axis simulated in FEMM is compared with the measured one. This comparison is used to understand if the needed mechanical accuracies are kept during the cooldown process.

The achieved mechanical accuracies are well inside the specified values as defined in [13].

IV. Results

This section presents the cool down, training, and magnetic field measurement results of the S-PRESSO mock-up. The half-period, peak field, and half-K parameter results (shown in

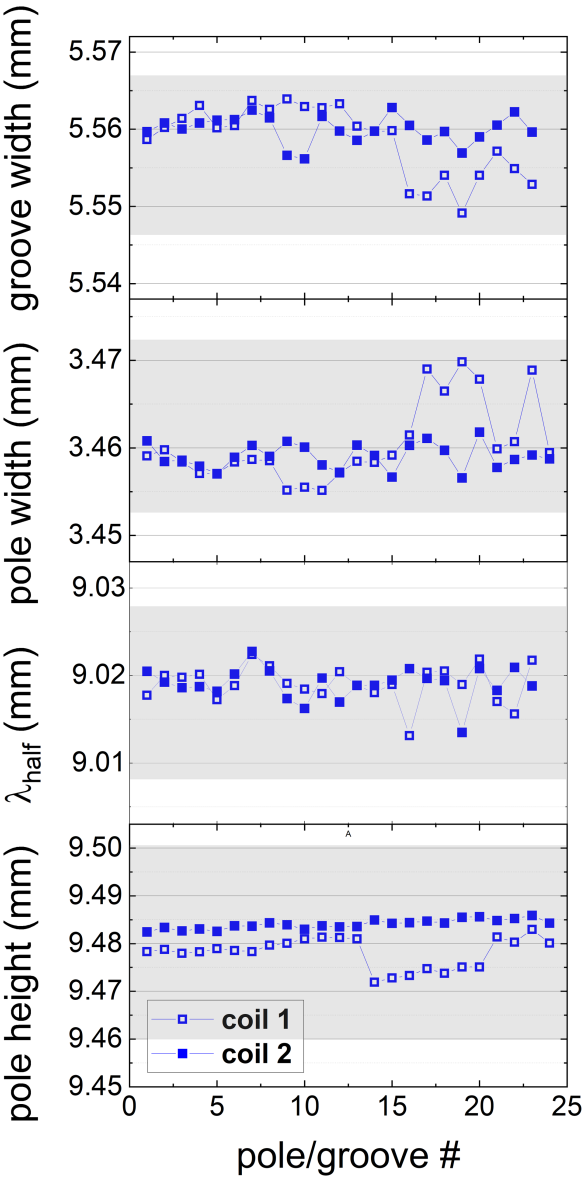

Fig. 6. Measured (blue squares) and specified (gray region) mechanical accuracy of Coils 1 and 2, excluding the influence of poles and grooves on end fields.

Section IV-E) are obtained as follows. For each absolute peak field, we exclude the end fields, and for the remaining peaks, the first and the last peaks are also removed, as illustrated in Fig. 7. The field is sampled with 100 μm steps. Unless otherwise stated, the currents in Aux1 and Aux2 are zero.

Let $B_{\text{peak}}[n]$ and $\hat{z}[n]$ be the absolute peak field of the field profile B and their corresponding locations along the longitudinal axis z. Let N be the total number of absolute peaks. The $N-1$ half-periods over the complete length are calculated by

$$\lambda_{\text{half}}[n] = \hat{z}[n+1] - \hat{z}[n],\ n = 1,2,3,\ldots,N-1. \quad (1)$$

The half-K parameter sequence is calculated by

$$K_{\text{half}}[n] = 93.36 B_{\text{peak}}[n] \times \lambda_{\text{half}}[n],\ n = 1,2,3,\ldots,N-1. \quad (2)$$

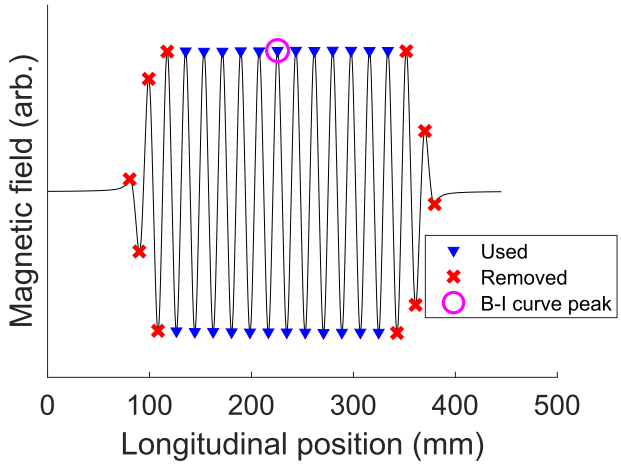

Fig. 7. Illustration of the absolute peak locations taken to calculate half-periods, peak field, and half-K parameter.

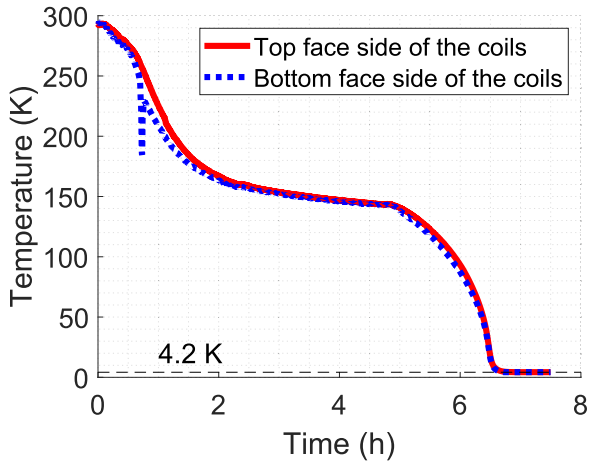

Fig. 8. Temperature profile inside the CASPER I cryostat during the first cool down.

Finally, we define $\Delta K_{\text{half}}/\overline{K_{\text{half}}}$ as the relative deviation of $K_{\text{half}}[n]$ with regard to its average $\overline{K_{\text{half}}}$, i.e.,

$$\frac{\Delta K_{\text{half}}}{\overline{K_{\text{half}}}} = \frac{K_{\text{half}}[n] - \overline{K_{\text{half}}}}{\overline{K_{\text{half}}}}. \quad (3)$$

The same pattern is used for the peak field and half-period, i.e., $\Delta B_{\text{peak}} = B_{\text{peak}}[n] - \overline{B_{\text{peak}}}$, $\Delta\lambda_{\text{half}} = \lambda_{\text{half}}[n] - \overline{\lambda_{\text{half}}}$, where the overline means the average over the whole sequence.

A. *Cool Down and Training*

Fig. 8 shows the temperature inside the cryostat during the cool down procedure. The procedure is divided into two phases. First, liquid Nitrogen cools the cryostat from room temperature to 150 K. After, liquid helium is used to reach 4.2 K. The complete cool down procedure took approximately 7 h. Two partial scans were performed for preliminary tests: one at room temperature and a second one at 150 K. For both preliminary scans, the current in the main coil was set to 200 mA.

The complete temperature profile during all the days of measurements is shown in Fig. 9. The number of quenches

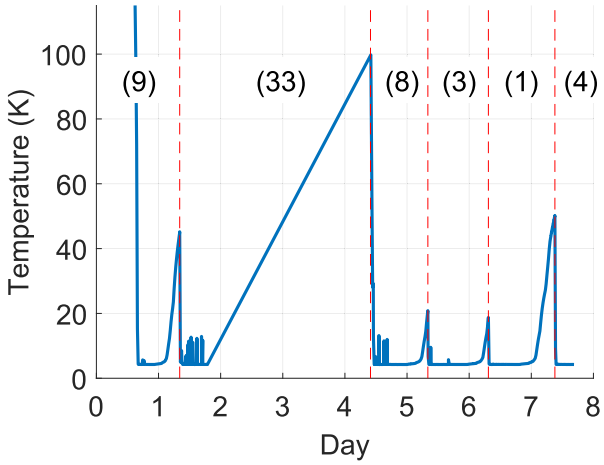

Fig. 9. Temperature profile inside the CASPER I cryostat during the complete measurement campaign. The number of quenches in between thermal cycles is shown in parentheses.

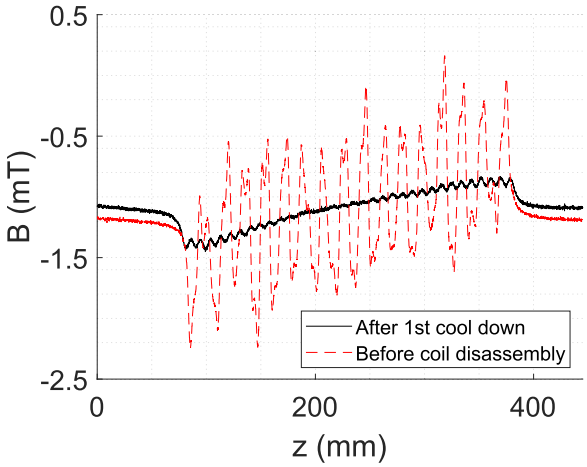

Fig. 11. Zero-current field measurement after first cool down and right before disassembling the coils.

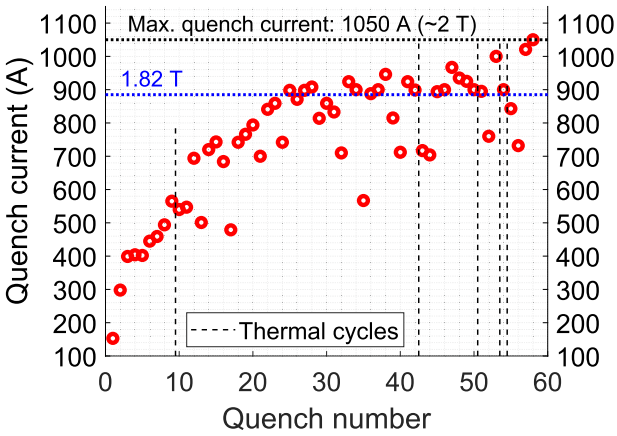

Fig. 10. S-PRESSO mock-up training.

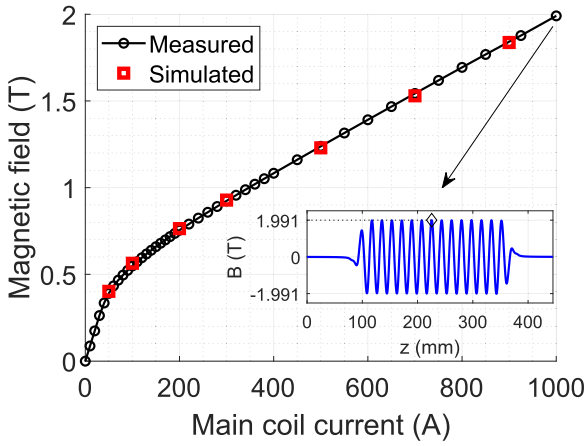

Fig. 12. Mock-up's B–I curve. The inset plot shows a full scan of the mock-up at 1000 A, reaching a peak field of approximately 2 T.

occurred during each thermal cycle is indicated in parentheses. The temperature rise from day 2 to day 4 are because those days were a weekend, i.e., there was no helium refill.

Fig. 10 shows the quench current during training. The maximum quench current was 1050 A — about 15% above the current of 885 A, which provides the nominal on-axis magnetic field of 1.82 T for a magnetic gap of 6.5 mm. The magnetic gap is determined by the height of the rails. The magnetic gap value at room temperature was measured down and upstream of the mock-up with a ceramic gauge block, resulting in 6.513 and 6.515 mm.

As a stability test, the coil was supplied with 900 A during 8 h without quenching. A full scan of the coils at 1000 A was also performed and the results are shown in Section IV-C.

B. Zero-Current Field

Fig. 11 presents the results of the zero-current field scans, performed after the first cool down and just before disassembling the coils. As expected, the post-measurement shows that the iron is more magnetized than it was before powering the coils to maximum current.

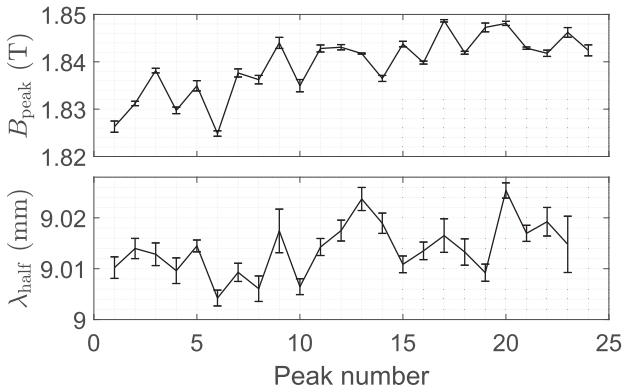

Fig. 13. Repeatability results of B_{peak} and λ_{half} from five scans at 900 A.

C. B–I Curve

We observed a good agreement between the measured and simulated peak field as a function of the main coil current. The correction coils had no current during the B–I curve measurements. The result is presented in Fig. 12. For each current, the

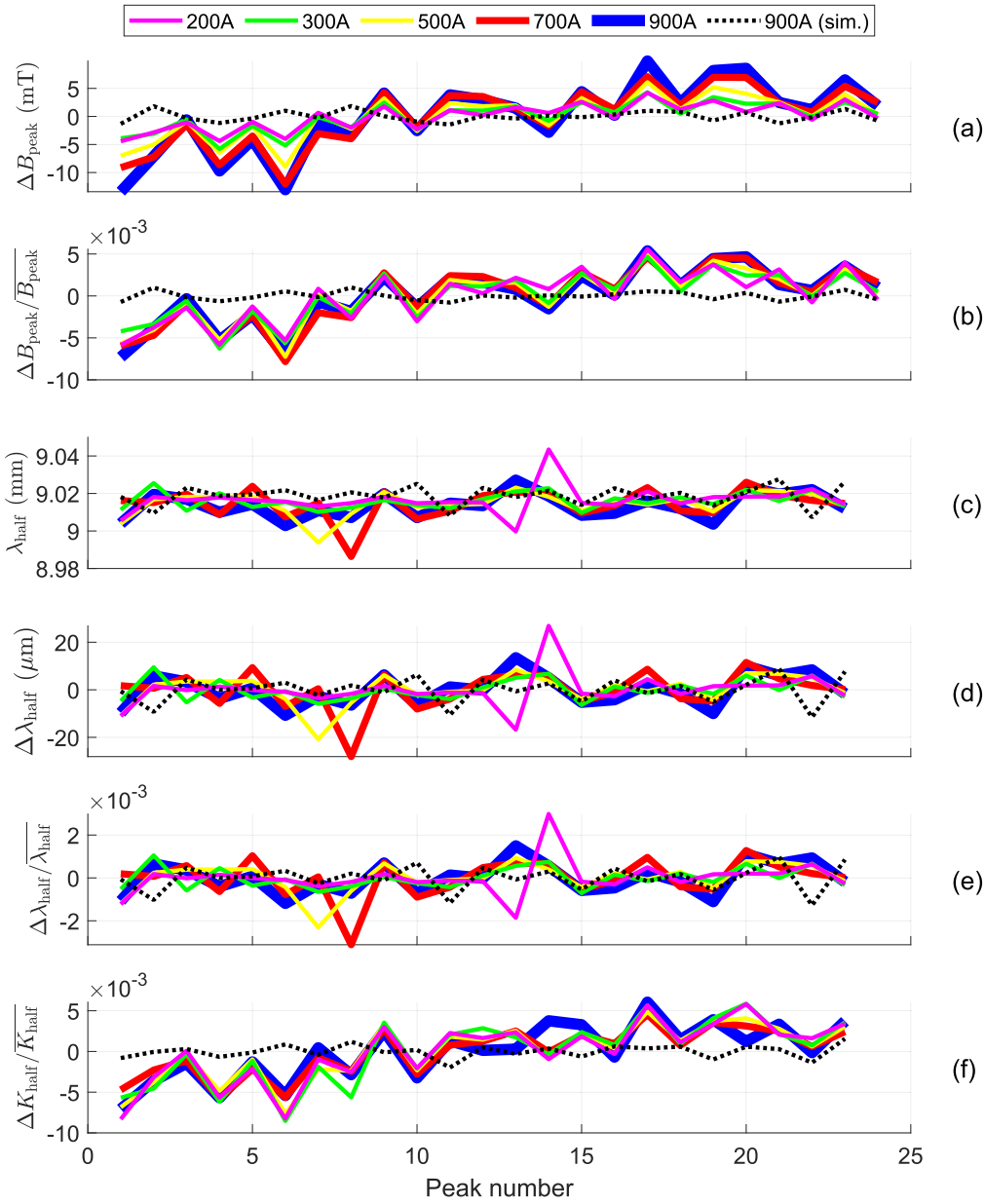

Fig. 14. (a) Peak field variation ΔB_{peak}, (b) peak field relative change $\Delta B_{\text{peak}}/\overline{B_{\text{peak}}}$, (c) half-period λ_{half}, (d) half-period variation $\Delta\lambda_{\text{half}}$, and (e) half-period relative change $\Delta\lambda_{\text{half}}/\overline{\lambda_{\text{half}}}$, and (f) half-K parameter relative change $\Delta K_{\text{half}}/\overline{K_{\text{half}}}$ among 200, 300, 500, 700, and 900 A currents in the main coil. The simulation for 900 A is also added. The current in Aux1 is indicated in Table I.

peak field is the maximum of a 1.5 mm scan performed around the middle pole (see Fig. 7 for a reference of the middle pole location). The inset in Fig. 12 shows a full scan at 1000 A, which reached approximately 2 T.

D. System's Repeatability

Five scans of the S-PRESSO mock-up were taken to evaluate the uncertanty of $B_{\text{peak}}[n]$, $\lambda_{\text{half}}[n]$, and $\text{rms}\{\Delta K_{\text{half}}[n]/\overline{K_{\text{half}}}\}$. The measurements were performed for a current of 900 A in the main coil. Fig. 13 shows the average peak field and half-period, respectively, among the five samples for each peak position and the error bar as the 95% of the confidence interval.

The variation among adjacent peaks and adjacent half-periods is larger than the error bars. Since the number of samples is small, we used the rms of the 95% of the confidence interval range to express the overall error, resulting in 1.5 mT for the peak field and 5 μm for the half-period. By propagating the error of the peak field and half-period, the relative uncertainty of the $\text{rms}\{\Delta K_{\text{half}}[n]/\overline{K_{\text{half}}}\}$ is less than 0.03%, indicating that the error in the measurements is approximately one three-thousandth of the measured value and reflecting the measuring system's high reliability and precision. Considering the mock-up under measurement's tight specifications, this level of relative uncertainty affirms the system's adequacy for tasks requiring high precision.

TABLE I
SIMULATED AND ACTUAL CURRENT OF THE AUX1 CORRECTION COIL TO CORRECT SECOND FIELD INTEGRAL FOR EACH CURRENT

Current in the Main Coil (A)	Simulated Current in the Correction Coil (A)	Simulated Second Field Integral (Tmm^2)	Actual Current in the Correction Coil Aux1 (A)
50	–0.07	+20	N.A.
100	+0.47	–13	N.A.
200	+1.17	+23	+1.37
300	+1.37	+24	+1.47
500	+1.67	+25	+1.78
700	+1.87	+32	+1.97
900	+1.97	–21	+2.07

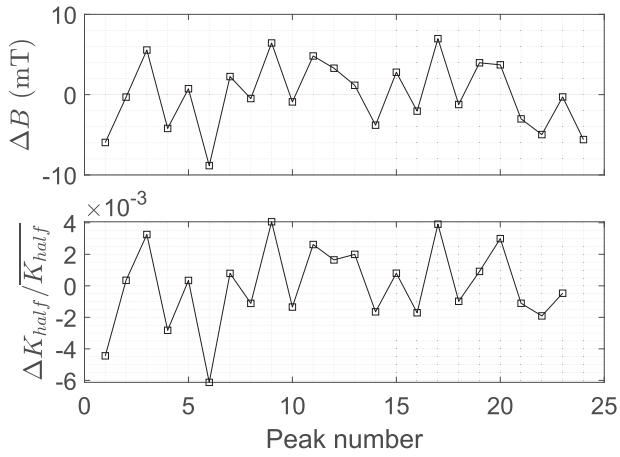

Fig. 15. Peak field variation and relative half-K parameter after detrending the peak fields.

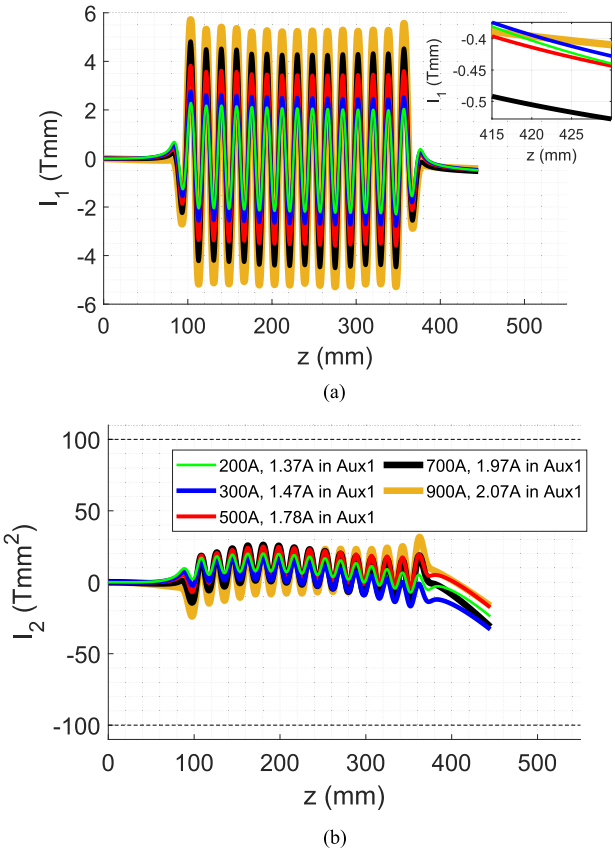

Fig. 16. (a) First and (b) second field integrals for 200, 300, 500, 700, and 900 A in the main coil. The current in Aux1 is indicated in the legend. The inset in (a) shows the first field integrals at the end of the coil. The first field integrals will be corrected using Helmholtz coils in the S-PRESSO coils. The dashed lines in (b) are the specified ± 100 Tmm^2 for the second field integral.

E. Half-Period, Absolute Peak Field, and Half-K Parameter Measurements

A complete scan was taken for five different currents in the main coil: 200, 300, 500, 700, and 900 A. Before the measurements, we simulated the required current in the correction coils to keep the second field integral within the specifications. The simulated current in the correction coil was the basis for setting the correction coils during the actual experiment. Table I gives the simulated results for the correction coil and the actual value set during the experiments.

Fig. 14 shows the peak field variation (ΔB_{peak}), the peak field relative change ($\Delta B_{\mathrm{peak}}/\overline{B_{\mathrm{peak}}}$), the half-period ($\lambda_{\mathrm{half}}$), the half-period variation ($\Delta\lambda_{\mathrm{half}}$), the half-period relative change ($\Delta\lambda_{\mathrm{half}}/\overline{\lambda_{\mathrm{half}}}$), and the half-K parameter relative change ($\Delta K_{\mathrm{half}}/\overline{K_{\mathrm{half}}}$).

Table II presents the statistics for each current in the main coil. The rms$\{\Delta K_{\mathrm{half}}/\overline{K_{\mathrm{half}}}\}$ is above the specification of 1.5×10^{-3}. Except for 300 A, the ranges are slightly above the required $\pm 6 \times 10^{-3}$. By detrending the tapering profile in the peak field, i.e., by removing their slope (also indicated in Table II), the rms$\{\Delta K_{\mathrm{half}}/\overline{K_{\mathrm{half}}}\}$ stays between 1.88×10^{-3} and 2.65×10^{-3}, while all the ranges are within $\pm 5.5 \times 10^{-3}$. Fig. 15 shows the detrended plot for 900 A (peak field and $\Delta K_{\mathrm{half}}/\overline{K_{\mathrm{half}}}$). The rms$\{\Delta K_{\mathrm{half}}/\overline{K_{\mathrm{half}}}\}$ for the detrended profile shown in Fig. 15 is 2.5×10^{-3}.

From the field profile at 900 A, a slope of 70 mT/m is observed. This can be explained by the following.

1) A tapering of about 75 μm over the coil length of 300 mm. As it can be calculated from [4], a change in gap of 75 μm corresponds to a change in the peak field of 21 mT.
2) a change of the Hall probe position along the magnetic axis toward the coils of 340 μm.

A combination of the abovementioned effects is also possible.

Fig. 14(b) shows that the winding positions are not modified by the magnetic forces. Otherwise, the relative variation would be more prominent for higher currents. The difference in the local variation observed in the peak field and half-period length comparing the simulations based on the geometry reached at room temperature indicates that the winding position (winding height) is changing in cold conditions. A similar effect was observed also in the 1.5 m long undulator coils with 20 mm period length installed now in the KIT synchrotron [14]. This might be improved by means of a stronger epoxy.

F. Field Integral Measurements

The first and second field integrals, I_1 and I_2, respectively, are shown in Fig. 16. The correction coil Aux1 allowed the mock-up second field integral to be kept within the specified

TABLE II
MAGNETIC FIELD STATISTICS FOR VARIOUS CURRENTS IN THE MAIN COIL

Current (A)	200	300	500	700	900
Magnetic field (T), meas.	0.55	0.75	1.24	1.54	1.84
RMS$\{\Delta K_{\text{half}}/\overline{K_{\text{half}}}\}(\times 10^{-3})$, meas.	3.37	2.88	3.38	3.85	3.73
RMS$\{\Delta K_{\text{half}}/\overline{K_{\text{half}}}\}(\times 10^{-3})$, sim.	0.56	0.79	0.84	0.84	0.81
Range$\{\Delta K_{\text{half}}/\overline{K_{\text{half}}}\}(\times 10^{-3})$, meas.	±6.57	±5.17	±6.27	±7.20	±7.07
Range$\{\Delta K_{\text{half}}/\overline{K_{\text{half}}}\}(\times 10^{-3})$, sim.	±1.24	±1.65	±1.90	±1.90	±1.77
RMS$\{\Delta \lambda_{\text{half}}/\overline{\lambda_{\text{half}}}\}(\times 10^{-3})$, meas.	0.81	0.48	0.71	0.90	0.72
RMS$\{\Delta \lambda_{\text{half}}/\overline{\lambda_{\text{half}}}\}(\times 10^{-3})$, sim.	0.49	0.56	0.60	0.60	0.59
Range$\{\Delta \lambda_{\text{half}}/\overline{\lambda_{\text{half}}}\}(\times 10^{-3})$, meas.	±2.42	±0.88	±1.62	±2.20	±1.34
Range$\{\Delta \lambda_{\text{half}}/\overline{\lambda_{\text{half}}}\}(\times 10^{-3})$, sim.	±0.77	±1.09	±1.16	±1.15	±1.13
RMS$\{\Delta B_{\text{peak}}/\overline{B_{\text{peak}}}\}(\times 10^{-3})$, meas.	3.11	2.83	3.10	3.41	3.33
RMS$\{\Delta B_{\text{peak}}/\overline{B_{\text{peak}}}\}(\times 10^{-3})$, sim.	0.43	0.56	0.58	0.55	0.51
Range$\{\Delta B_{\text{peak}}/\overline{B_{\text{peak}}}\}(\times 10^{-3})$, meas.	±5.72	±5.47	±6.09	±6.23	±6.34
Range$\{\Delta B_{\text{peak}}/\overline{B_{\text{peak}}}\}(\times 10^{-3})$, sim.	±0.89	±1.16	±1.14	±1.02	±0.90
$\overline{\lambda_{\text{half}}}$ (mm), meas.	9.017	9.016	9.015	9.015	9.014
$\overline{\lambda_{\text{half}}}$ (mm), sim.	9.019	9.019	9.019	9.019	9.019

The current in Aux1 is indicated in Table I. The numbers are calculated from measured (meas.) and simulated (sim.) results. The measured magnetic field is taken from the pole indicated in Fig. 7.

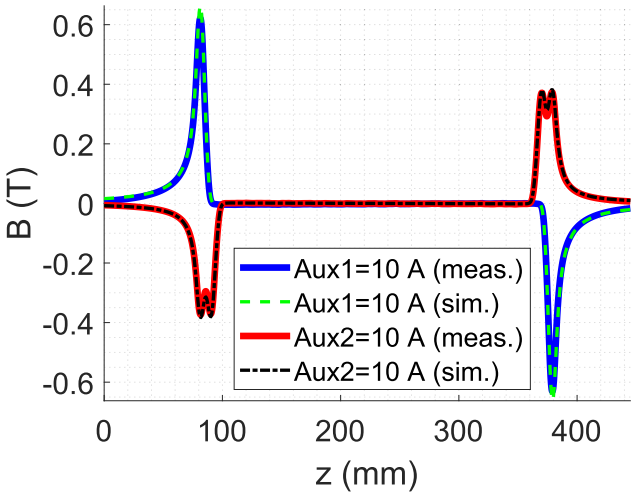

Fig. 17. Magnetic field profile (measured and simulated) from the correction coils. When Aux1 is powered with 10 A, Aux2 is zero; when Aux2 is powered with 10 A, Aux1 is zero.

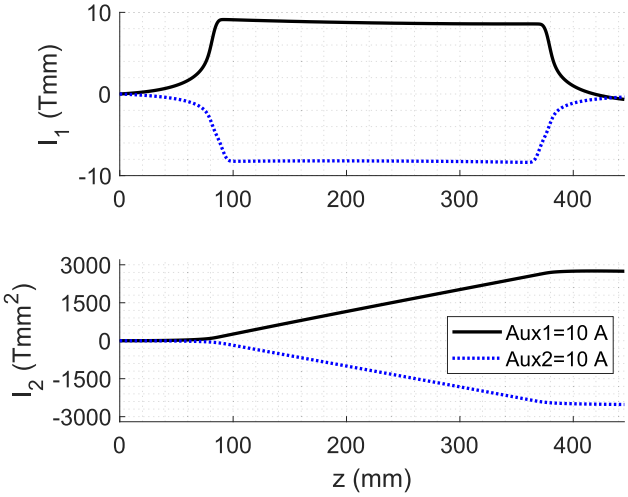

Fig. 18. Measured field integral profiles from the correction coils. When Aux1 is powered with 10 A, Aux2 is zero; when Aux2 is powered with 10 A, Aux1 is zero.

value of 100 Tmm^2. The first field integral can be corrected with Helmholtz coils (not installed for the test campaign reported in this article). Maintaining a flat trajectory is crucial for the FEL performance, as it ensures the proper spatial overlap of photons.

The field integrals for S-PRESSO will be characterized in the SUNDAE2 magnetic measurement test stand with the moving wire technique [7].

G. Correction Coil Measurements

To measure the correction coils contribution, we scanned the magnetic field after setting the current of one of the Aux1 and Aux2 correction coils to 10 A while keeping the other one at zero. The main coil current was always zero. The magnetic field generated from Aux1 and Aux2 are shown in Fig. 17. Fig. 18 presents the first and second field integrals for the measured profiles shown in Fig. 17. As shown in the figures, Aux1 and Aux2 have the same functionality.

V. CONCLUSION

In this study, we investigated the manufacturing and assembly quality of the S-PRESSO SCU mock-up tested in the CASPER I facility at the IBPT at KIT. The design and manufacturing procedures have been proven to be solid. The mock-up reached a current of 1050 A, which corresponds to the calculated crossing point between the load line and superconducting wire critical current at 4.2 K (short sample limit). A stability test demonstrated that the mock-up could sustain a current of 900 A for 8 h without quenching.

The tests performed had also a particular emphasis on evaluating a sledge designed and produced by European XFEL that holds the Hall probe and travels through the mock-up's gap. The same sledge is planned to be used in the SUNDAE1 test stand facility, under development at European XFEL. The end fields design is sound and the correction coils successfully kept the second field integral well within the specified ± 100 Tmm^2 range. This is of utmost importance to ensure the spatial overlap

of the constructively interfering photons along the undulator length, and consequently, high flux. However, rms values for $\Delta K_{\text{half}}/\overline{K_{\text{half}}}$ were approximately double the specified target. Furthermore, a tapering effect in the peak field profiles is observed. The source of the observed tapering effect in the field could come from the mock-up assembly quality or from the mechanical accuracy of the rails. This aspect warrants further investigation.

These results demonstrate the robustness of the magnetic design of S-PRESSO that will be installed and tested in the European XFEL.

ACKNOWLEDGMENT

The authors would like to thank Bennet Krasch, Nicole Glamann, and David Saez de Jauregui from the Institute for Beam Physics and Technology at KIT for their technical support.

REFERENCES

[1] K. Zhang and M. Calvi, "Review and prospects of world-wide superconducting undulator development for synchrotrons and FELs," *Supercond. Sci. Technol.*, vol. 35, no. 9, Jul. 2022, Art. no. 093001, doi: 10.1088/1361-6668/ac782a.

[2] D. Nguyen et al., "Superconducting undulators and cryomodules for X-ray free-electron lasers," in *Proc. 5th Int. Part. Accel. Conf.*, 2022, pp. 870–873. [Online]. Available: https://jacow.org/napac2022/papers/thye3.pdf

[3] Q. Tang et al., "Cooling design for the magnetic structure of SHINE superconducting undulator," *IEEE Trans. Appl. Supercond.*, vol. 30, no. 4, Jun. 2020, Art. no. 4100104.

[4] S. Casalbuoni et al., "Superconducting undulator activities at the European X-ray free-electron laser facility," *Front. Phys.*, vol. 11, 2023, Art. no. 1204073, doi: 10.3389/fphy.2023.1204073.

[5] S. Casalbuoni et al., "A pre-series prototype for the superconducting undulator afterburner for the European XFEL," *J. Phys.: Conf. Ser.*, vol. 2380, no. 1, Dec. 2022, Art. no. 012012, doi: 10.1088/1742-6596/2380/1/012012.

[6] B. Marchetti et al., "Conceptual design of a liquid helium vertical test-stand for 2 m long superconducting undulator coils," *J. Phys.: Conf. Ser.*, vol. 2380, no. 1, Dec. 2022, Art. no. 012027, doi: 10.1088/1742-6596/2380/1/012027.

[7] J. Baader et al., "Status update on SUNDAE2 magnetic field test facility at European XFEL," in *Proc. 14th Int. Part. Accel. Conf.*, 2023, pp. 1215–1218. [Online]. Available: https://indico.jacow.org/event/41/contributions/976

[8] E. Mashkina et al., "Casper- a magnetic measurement facility for superconducting undulators," *J. Phys.: Conf. Ser.*, vol. 97, no. 1, Feb. 2008, Art. no. 012020, doi: 10.1088/1742-6596/97/1/012020.

[9] L. Bottura, "A practical fit for the critical surface of NbTi," *IEEE Trans. Appl. Supercond.*, vol. 10, no. 1, pp. 1054–1057, Mar. 2000.

[10] B. Marchetti, S. Casalbuoni, V. Grattoni, and S. Serkez, "Analysis of the error budget for a superconducting undulator SASE line at European XFEL," *J. Phys.: Conf. Ser.*, vol. 2380, no. 1, Dec. 2022, Art. no. 012011, doi: 10.1088/1742-6596/2380/1/012011.

[11] "Opera 3d," Accessed on: Nov. 30, 2023. [Online]. Available: https://www.3ds.com/products-services/simulia/products/opera/

[12] "FEMM - finite element method magnetics," Accessed on: Nov. 29, 2023. [Online]. Available: https://www.femm.info/

[13] V. Grattoni, S. Casalbuoni, and B. Marchetti, "An analytical study to determine the mechanical tolerances for the afterburner superconducting undulators at EuXFEL," *J. Phys.: Conf. Ser.*, vol. 2380, no. 1, Dec. 2022, Art. no. 012010, doi: 10.1088/1742-6596/2380/1/012010.

[14] S. Casalbuoni et al., "Field quality of 1.5 m long conduction cooled superconducting undulator coils with 20 mm period length," *J. Phys.: Conf. Ser.*, vol. 874, no. 1, Jul. 2017, Art. no. 12015, doi: 10.1088/1742-6596/874/1/012015.